Nuclear Engineering and Technology 54 (2022) 4474–4480

Contents lists available at ScienceDirect

Nuclear Engineering and Technology

journal homepage: www.elsevier.com/locate/net

Original Article

Corrosion behaviors of SS316L, Ti-Gr.2, Alloy 22 and Cu in KURT groundwater solutions for geological deep disposal

Gha-Young Kim [a, *], Junhyuk Jang [a], Minsoo Lee [a], Mihye Kong [a], Seok Yoon [b]

[a] Disposal Performance Demonstration Research Division, Korea Atomic Energy Research Institute, Daedeok-daero 989-111, Yuseongu, Daejeon, 34057, South Korea
[b] Disposal Safety Evaluation Research Division, Korea Atomic Energy Research Institute, Daedeok-daero 989-111, Yuseongu, Daejeon, 34057, South Korea

ARTICLE INFO

Article history:
Received 16 February 2022
Received in revised form
6 July 2022
Accepted 25 July 2022
Available online 2 August 2022

Keywords:
Canister
Corrosion
Geological deep disposal
KAERI underground research tunnel
groundwater
Polarization
Impedance

ABSTRACT

Deep geological disposal using a multibarrier system is a promising solution for treating high-level radioactive (HLRW) waste. The HLRW canister represents the first barrier for the migration of radionuclides into the biosphere, therefore, the corrosion behavior of canister materials is of significance. In this study, the electrochemical behaviors of SS316L, Ti-Gr.2, Alloy 22, and Cu in naturally aerated KAERI underground research tunnel (KURT) groundwater solutions were examined. The corrosion potential, current, and impedance spectra of the test materials were recorded using electrochemical methods. According to polarization and impedance measurements, Cu exhibits relatively higher corrosion rates and a lower corrosion resistance ability than those exhibited by the other materials in the given groundwater condition. In the anodic dissolution tests, SS316L exposed to the groundwater solution exhibited the most uniform corrosion, as indicated by its surface roughness. This phenomenon could be attributed to the extremely low concentration of chloride ions in KURT groundwater.

1. Introduction

Many countries worldwide have examined deep geological disposal systems with multiple barriers as a promising solution for the treatment of high-level radioactive waste (HLRW). Because HLRW containers (i.e., canisters) represent the first barrier to the migration of radionuclides into the biosphere, the corrosion behavior of suitable corrosion-resistant materials must be examined during canister selection. Also the buffer, which is filling material into a gap between canister and disposal borehole, can be eroded so that advective conditions prevail in the deposition hole. As advective conditions at the canister surface can lead to enhanced corrosion, it is necessary to select corrosion-resistant materials for the safety assessment [1]. In this reason, several candidate materials for canisters, such as nickel alloys, stainless and carbon steels, titanium alloys, and copper, have been studied [1–5].

Because Ni-based alloys form a thin chemically impervious surface oxide, they exhibit exceptional corrosion resistance and are used in a wide range of industrial applications. This corrosion resistance is attributable to Cr and Mo, Cr resists corrosion in oxidizing acids and maintains passivity, and Mo enhances the corrosion resistance against reducing acids [6]. Among Ni–Cr–Mo alloys, alloy 22 (Ni–22Cr–13Mo–3W–4Fe) has been used as a reference material for fabricating nuclear waste packages in Yucca Mountain, Nevada, USA. Stainless steels, which are Fe–Cr alloys containing at least 11–13 wt% Cr, have a passive nature, resulting in low rates of general corrosion. However, the use of these materials is limited owing to their inferior performance in chloride environments. Carbon steels (Fe–C alloys) have been employed in many countries (Belgium, France, Switzerland, and Japan) owing to their excellent corrosion resistance, sufficient structural strength, and established fabrication methods. However, the production of H_2 and Fe(II) during anaerobic corrosion adversely influences the performances and properties of other barriers [7]. Ti alloys with low density and high strength were considered promising canister materials in Sweden, Japan, and Canada [8]. Moreover, these alloys were recommended to be used in preparing drip shields in the US Yucca Mountain Project [9]. Oxygen-free copper is a promising candidate for designing HLRW containers owing to its excellent resistance to general and localized corrosion in aqueous electrolytes, particularly in reducing environments, such as repository sites [10]. Pure copper with an oxygen content of less than 5 ppm

* Corresponding author.
E-mail address: gkim@kaeri.re.kr (G.-Y. Kim).

https://doi.org/10.1016/j.net.2022.07.024

exhibits minimized segregation at grain boundaries and can be doped with phosphorous to increase creep resistance [11]. This material has been used for preparing metallic engineered barriers in deep geological repositories for HLRW in Finland and Sweden.

Overall, extensive research has been conducted to select materials for building canisters. Notably, canister corrosion behavior is highly dependent on the characteristics of repository sites, e.g. ground water composition, which may vary significantly for different types of geology. In this context, it is necessary to study the corrosion behaviors of canister materials in Korean domestic repository environments. To this end, this study was aimed at comparing the corrosion behaviors of candidate canister materials SS316L, Ti-Gr.2, Alloy 22, and Cu in KAERI underground research tunnel (KURT) groundwater solutions. Potentiodynamic polarization and electrochemical impedance spectroscopy (EIS) analyses were performed to determine the corrosion potential, current, and resistance of the test materials. Furthermore, anodic dissolution tests were conducted to examine the corrosion uniformity for these materials.

2. Material and methods

Stainless steel grade AISI 316L (SS316L), titanium grade 2 (Ti-Gr.2), Ni alloy 22 (Alloy 22), and oxygen-free phosphorous-micro-alloyed Cu (procured from Swedish Nuclear Fuel and Waste Management Co.) were used as the working electrodes. Table 1 summarizes the chemical compositions of the test materials. All working electrodes were disk-type (diameter and thickness of 15 and 1 mm, respectively) and the exposed surface area was 1 cm^2. Prior to the electrochemical tests, the electrodes were abraded with a series of silicon carbide papers (up to 2000 grit), polished to a mirror finish using 0.15-μm alumina paste, ultrasonically treated in distilled water for 5 min, and dried. A saturated calomel reference electrode (SCE) and a Pt-mesh counter electrode were used to assemble the cell for the potentiodynamic and EIS measurements. For the dissolution tests, graphite rods were used as the counter electrode instead of Pt. All potentials are presented on the SCE scale. The electrolyte solution was derived from KURT groundwater. The sampled groundwater was naturally ejected from a hole at a depth of 150 m at location #RG-1 in KURT. The chemical composition of KURT groundwater is listed and compared with Sweden in Table 2 [12]. Note that the ratio of chloride/carbonate in KURT groundwater is lower than that in Swedish groundwater. The inorganic elements were analyzed using a Thermo Scientific iCAP7400 duo inductively coupled plasma atomic emission spectroscopy instrument (Waltham, MA). The anions, except bicarbonate ions, were analyzed using a Metrohm ion chromatograph. The KURT groundwater (pH 7.91) was vacuum filtered with 1-μm pore-size cellulose filter paper before being used in electrochemical measurements.

A BioLogic SP-300 potentiostat/galvanostat was used to conduct the electrochemical experiments with a typical three-electrode cell configuration. All experiments were conducted at room temperature (25 °C). Potentiodynamic polarization curves were obtained for the comparative analysis of the test materials in the initial stage of immersion, with a scan rate of 1 mV/s in the range of −0.5 to 1.0 V vs. open circuit potential (OCP; E_{oc}). Before the polarization measurements, the OCP of the electrodes in the solution was monitored until it stabilized (after approximately 2 h). The potentiodynamic experiments were repeated three times. EIS measurements were performed at OCP, applying an AC signal of ±10-mV rms amplitude, in a frequency range of 100 kHz to 10 mHz, and the sampling size was six data points per decade. Anodic dissolution tests were performed by applying a constant current (10 mA/cm^2) for 24 h to observe the surface changes of the materials. After dissolution, the test coupons were washed with deionized water and dried. Subsequently, the surface roughness of the materials was measured using a contact surface profiler (P-7 Stylus Profiler, KLA-Tencor, San Jose, CA).

3. Results and discussion

The electrochemical behavior of the test materials was investigated using potentiodynamic measurements. The polarization curves for SS316L, Alloy 22, and Cu, exposed to stagnant and naturally aerated KURT groundwater (blank solution), are shown in Fig. 1a. The polarization curve of Ti-Gr.2 could not be measured owing to the high overload possibly induced by the pitting of passive titanium oxide film [13]. In the KURT groundwater solution, Cu exhibited anodic behavior with a relatively positive corrosion potential (E_{CORR}, −0.047 V vs. SCE) and higher corrosion current density (i_{CORR}, 0.938 $\mu A/cm^2$) compared to the other materials. As the electrode potential increased to more than the E_{CORR}, the anodic current of Cu increased in a two-step manner, corresponding to the anodic dissolution of $Cu \rightarrow Cu^{+} \rightarrow Cu^{2+}$. SS316L exhibited E_{CORR} and i_{CORR} values of −0.198 V vs. SCE and 0.124 $\mu A/cm^2$, respectively. The current density gradually increased with the potential and stabilized at 0.4 V vs. SCE. Alloy 22 exhibited an E_{CORR} value of −0.175 V vs. SCE, and the i_{CORR} value gradually increased with the potential. When sulfate ions were introduced in the groundwater solution, the corrosion behaviors of the materials were altered, as

Table 1
Composition of test materials used in this study.

Chemical composition (%)	SS316L	Ti-Gr.2	Alloy 22	Cu
C	0.030 max	0.08 max	0.015 max	–
Si	1.00 max	–	0.08 max	–
Mn	2.00 max	–	0.50 max	–
P	0.45 max	–	0.02 max	0.005
S	0.030 max	–	0.02 max	<0.0008
Cr	16.0–18.0	–	20.0–22.5	–
Mo	2.00–3.00	–	12.5–14.5	–
Fe	Remainder	0.25 max	2.0–6.0	–
Ni	10.00–15.00	–	Remainder	–
Ti	–	Remainder	–	–
Cu	–	–	–	Remainder
Co	–	–	2.5–3.5	–
W	–	–	2.5 max	–
V	–	–	0.35 max	–
N	–	0.03 max	–	–
H	–	0.013 max	–	–
O	–	0.20 max	–	0.0005

Table 2
Composition of KAERI underground research tunnel (KURT) groundwater and Sweden Forsmark-North Uppland area (*Measured chemical composition of the groundwater used in this study, **Estimated chemical composition of the groundwater at the repository depth [12]).

		KAERI Underground Research Tunnel (KURT) site*	Sweden Forsmark-North Uppland area **
Depth [m]		150	500
Eh [mV]		350	0 to −280
pH		7.91	6 to 9
[mg/L]	Na^+	8.2	90 to 3750
	K^+	0.48	1 to 136
	Ca^{2+}	19	58 to 1900
	Mg^{2+}	1.4	0.1 to 460
	HCO_3^-	54.8	5 to 290
	SO_4^{2-}	4.3	19 to 900
	Cl^-	3.1	95 to 6900
	HS^-	–	0 to 0.3

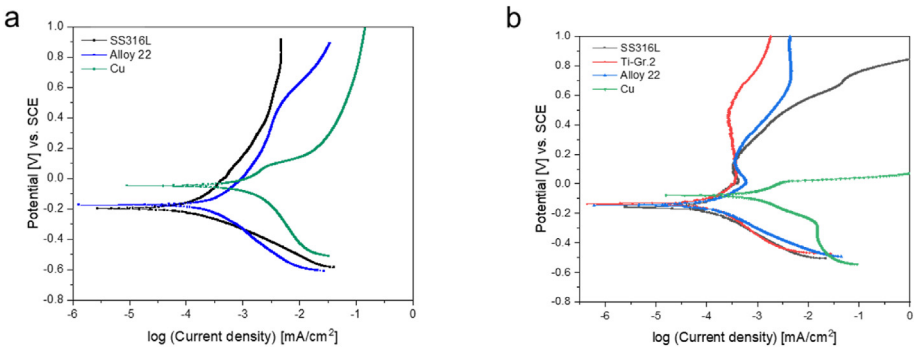

Fig. 1. Potentiodynamic scans of SS316L, Ti-Gr.2, Alloy 22, and Cu in naturally aerated KURT groundwater (a) without and (b) with the addition of 0.1-M Na_2SO_4 (scan rate = 1 mV/s, 25 °C).

shown in Fig. 1b. The anodic corrosion current densities of SS316L, Ti-Gr.2, and Alloy 22 exhibited similar limiting values after an initial polarization ΔE of 0.16–0.17 V, and the E_{CORR} values were noted to be in a similar range. Ti-Gr.2 and Alloy 22 exhibited a passive region that extended to 1.0 V vs. SCE. In contrast, the anodic current density continuously increased in the case of SS316L. The addition of sulfate ions to the groundwater solution did not significantly change the corrosion current densities of the test materials. Notably, the corrosion potential of SS316L and Alloy 22 shifted to more positive values. In contrast, the E_{CORR} of Cu shifted to the negative direction. The anodic current density of Cu sharply increased as the anodic potential scan proceeded. These findings indicated that the presence of sulfate ions hindered the passivation of SS316L and Cu [14].

EIS measurements at OCP were obtained with the test materials exposed to the KURT groundwater solution. The experimental impedance spectra are presented in the form of Nyquist and Bode plots in Fig. 2. A complete capacitive loop with no tail (i.e., Warburg impedance) was observed when SS316L, Ti-Gr.2, and Alloy 22 were exposed to a blank solution (Fig. 2a). The impedance spectra of Cu in the KURT groundwater solution exhibited a tail corresponding to the Warburg impedance in the low-frequency region of the Nyquist diagram, suggestive of the occurrence of diffusion-controlled corrosion on the Cu surface. It may be related with vacancy diffusion through the Cu_2O film or diffusion of Cu(II) to the surface, which is an intermediate/secondary oxidant for Cu when Cu corrodes by O_2 as primary oxidant [12]. In general, the diameter of the semicircle arc can be used to characterize the corrosion resistance behavior of materials immersed in solutions. Larger diameters of the semicircle arc correspond to a higher corrosion resistance of the oxide film formed in solution [15]. Therefore, the corrosion resistance of the test materials immersed in the KURT groundwater solution exhibited the following order: SS316L > Alloy 22 > Ti-Gr. 2 > Cu, which is almost coincided with the total impedance value in Fig. 2b. At high frequencies, between 1000 and 100 Hz, EIS Bode plots can indicate the total impedance associated with the solution resistance (R_s) at the metal–electrolyte interface and help clarify the electrochemical corrosion process [16]. In this study, more than one order of difference in R_s was observed, and the value was higher in blank KURT groundwater than that in sulfate-added solutions. In other words, groundwater with a smaller content of ionic elements exhibited a low conductivity. The impedance magnitudes between 1 and 0.01 Hz could be attributed to the electrochemical corrosion occurring on the metal surface (i.e., the formation of several corrosion products) [16]. The lowest impedance magnitude in this range corresponded to Cu for solutions involving and not involving sulfate ions, indicating the relatively low corrosion resistance of Cu in this experiment. The phase maxima appeared in the low-frequency range, likely because of the presence of the protective oxide film (Fig. 2c). Fig. 2d presents the Nyquist plots for the SS316L, Ti-Gr.2, Alloy 22, and Cu surfaces exposed to a 0.1-M Na_2SO_4–added groundwater solution. The Nyquist diagrams of SS316L and Ti-Gr.2 indicated an incomplete capacitive reactance arc, attributable to the double-layer capacitance and charge transfer resistance of the surface. The impedance responses of Alloy 22 and Cu exhibited the form of a semicircle followed with a slash in the low-frequency region. In the frequency range of 1–0.01 Hz, the total impedance of Cu was considerably lower than those of the other materials (Fig. 2e). This finding shows that the Cu surface is more susceptible to general corrosion than the other materials under this condition. The highest total impedance in the sulfate-added groundwater solution corresponded to Ti-Gr.2, followed by SS316L and Alloy 22. This finding was consistent with the results shown in Fig. 2d. As shown in Fig. 2f, an additional peak of the

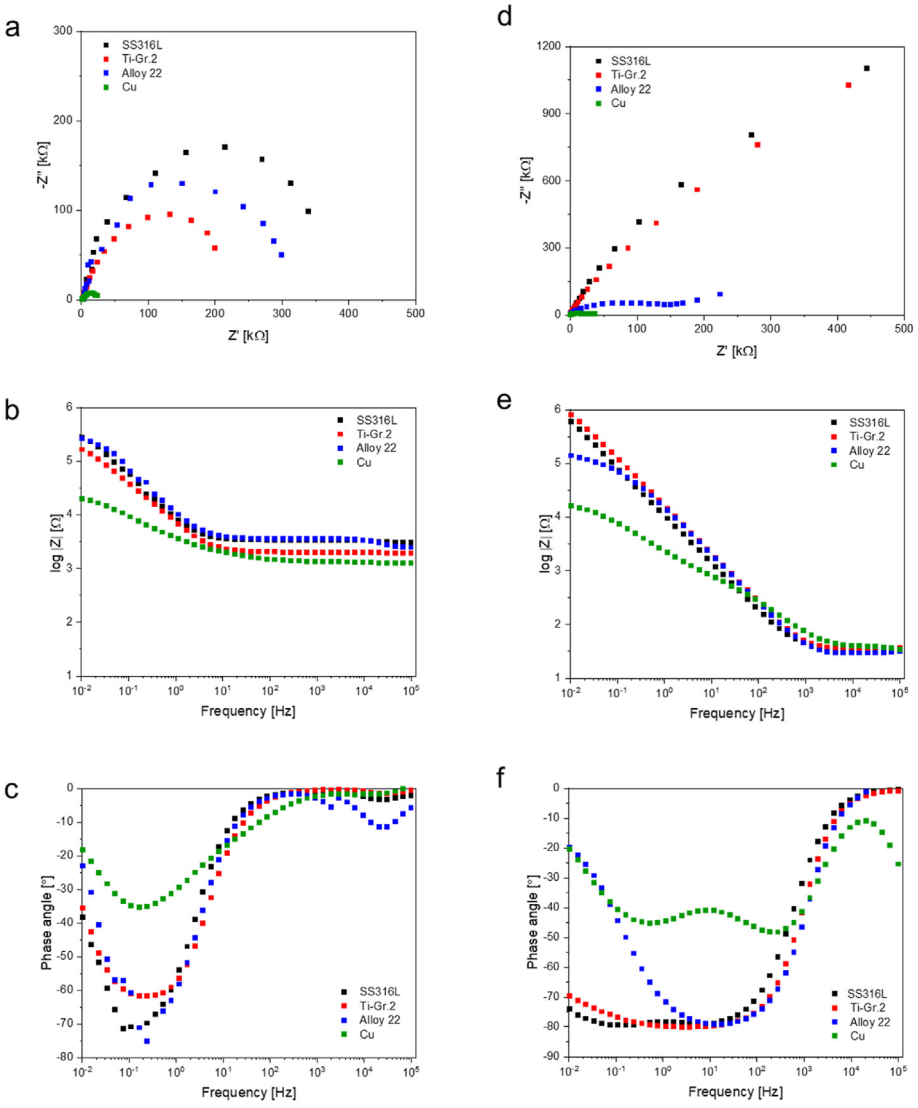

Fig. 2. Nyquist (a,d) and Bode (b,c,e,f) plots of SS316L, Ti-Gr.2, Alloy 22, and Cu in naturally aerated KURT groundwater (a–c) without and (d–f) with 0.1-M Na_2SO_4 at 25 °C.

phase angle appeared for SS316L and Cu; the highest phase angle shift corresponded to Alloy 22; and the phase angle for Ti-Gr.2 exhibited broadening. These changes were observed in the intermediate frequency range (100–1 Hz). Phase angle values of approximately −80° over the wide range of frequencies indicated that a stable passive film was formed on the surface of SS316L and Ti-Gr.2 while the electrodes were immersed in the sulfate-added KURT groundwater solution to perform EIS measurement [17].

The measured impedance data in the KURT groundwater solution were fitted using equivalent circuits, as shown in Fig. 3, to quantify and compare the impedance components of the test materials. The equivalent circuits are mostly used to elucidate the obtained data [18,19]. The fitted curves are shown in Fig. 4. In the equivalent circuits, R refers to the resistance element and Q is the constant phase element (CPE) adopted to represent nonideal capacitive behavior owing to uneven current distribution or surface inhomogeneity. The CPE can be defined as $Z_{CPE} = [Q(j\omega)^n]^{-1}$ ($j^2 = -1$), where Q is the CPE amplitude, ω the angular frequency, and n the CPE exponent [20]. The parameters Q and n are independent of the frequency. The value of n can be $0 \leq n \leq 1$, where 1 and 0 correspond to ideal capacitors and resistors, respectively. Table 3 lists the values of parameters deduced from the fits of the EIS spectra to the equivalent circuit. The RC combination observed at the metal surface in contact with the solution could be attributed to (i) the double-layer capacitance with charge transfer resistance [21–27] and (ii) the oxide film capacitance with resistance

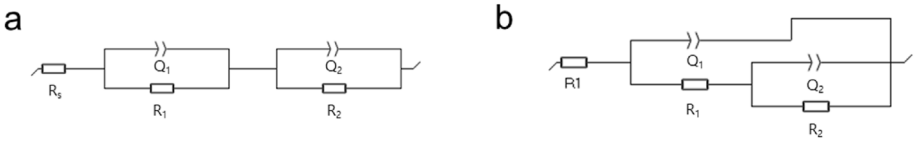

Fig. 3. Equivalent circuits used to fit EIS spectra in sulfate-added KURT groundwater solution for (a) SS316L, Ti-Gr.2, and Alloy 22, and (b) Cu.

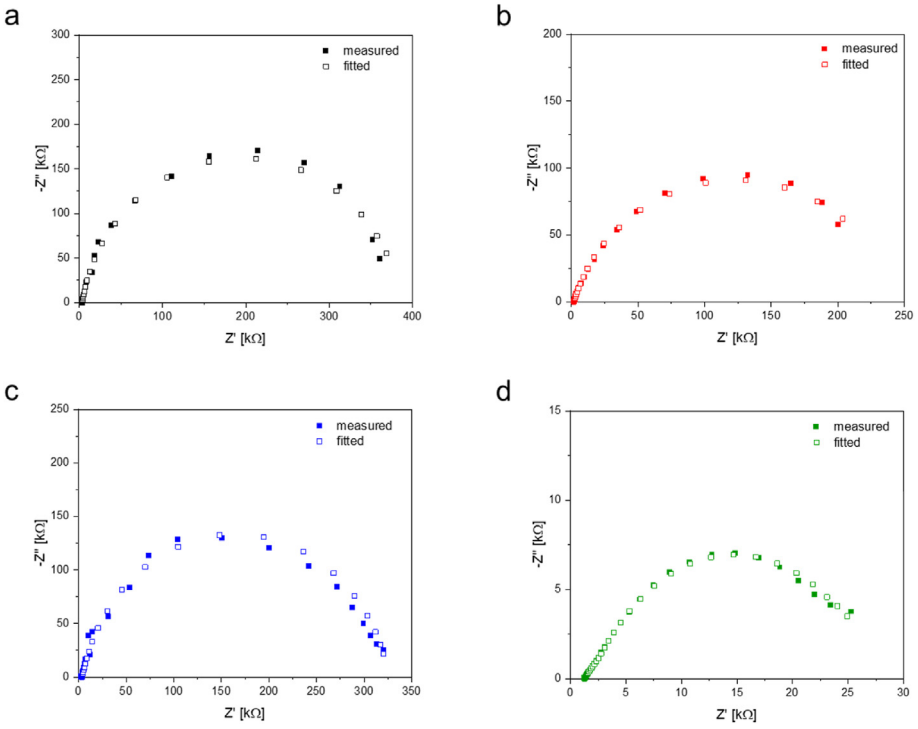

Fig. 4. Measured and fitted impedance of (a) SS316L, (b) Ti-Gr.2, (c) Alloy 22, and (d) Cu in sulfate-added KURT groundwater solution at 25 °C.

Table 3
Fitting parameters obtained from EIS measurements for SS316L, Ti-Gr.2, Alloy 22, and Cu immersed in naturally aerated KURT groundwater solution at 25 °C.

	SS316L	Ti-Gr.2	Alloy 22	Cu
R_s [kΩ·cm^2]	2.94	1.88	3.49	1.27
Q_1 [μF·s$^{(n1-1)}$ ·cm^{-2}]	26.7	0.05	19.4	82.3
n_1	0.894	1.000	0.882	0.575
R_1 [kΩ·cm^2]	383.3	0.055	321.5	3.43
Q_2 [μF·s$^{(n2-1)}$ ·cm^{-2}]	0.09	35.1	62.2	55.2
n_2	0.849	0.818	1.000	0.717
R_2 [kΩ·cm^2]	0.43	243.0	1.00	23.4

experienced by the ions while traveling through the oxide [28–33]. Notably, despite the significant research on metals immersed in solutions, the interpretation of the physical meaning of RC combinations in a circuit is different in various studies. In general, the first time constant ($Q_1//R_1$) could be attributed to factors (i) or (ii), and the meaning of $Q_2//R_2$ differs depending on the assignment of $Q_1//R_1$ [21]. Therefore, in this study, instead of comparing each impedance element, the polarization resistance (R_p) was calculated [33,34]: $R_p = R_b + R_{ct}$, where R_b is the resistance of corrosion product layer and R_{ct} is the charge transfer resistance. In the given framework, R_p was calculated as the sum of R_1 and R_2, and the calculated values are listed in Table 4. The polarization resistance of Cu is one order lower than those of the other materials, consistent with the results of the Bode plot (|Z| value) shown in Fig. 2b.

To examine the corrosion uniformity of the test materials based on the electrochemical reaction, anodic dissolution tests were performed in a 0.1-M Na_2SO_4–added KURT groundwater solution with an applied current of 10 mA/cm^2 for 24 h. In this artificially induced corrosion environment, the value was 10^4 times higher than that in the normal condition, based on the i_{CORR} of Cu in KURT groundwater (~1 μA/cm^2), as shown in Fig. 1a. Fig. 5a–c show the potential profiles of the test materials during the anodic dissolution. The dissolution test of Ti-Gr.2 was not conducted owing to the high overpotential of titanium, as in the case of the polarization measurement. The potential values of the test materials increased as the reaction progressed because of the overpotential induced by the generation and accumulation of corrosion products on the metal surface. In the case of Cu, the potential reached 0.1 V vs. SCE, consistent with the observations of the polarization curve (Fig. 1b). The surface roughness profiles of the materials after the dissolution test are shown in Fig. 5d–f. The lowest and highest deviations in the roughness corresponded to SS316L (average roughness, R_a = 0.72 μm) and Alloy 22 (R_a = 8.8 μm), respectively. Cu (R_a = 6.7 μm) exhibited a roughness intermediate to those of the two materials. The SS316L surface immersed in the test groundwater solution exhibited the most uniform corrosion, indicated by the lowest deviation in the surface roughness (Fig. 5d). Although SS316L and Alloy 22 are known to be vulnerable to local corrosion, no traces of local corrosion were observed. This phenomenon likely occurred owing to the negligible concentration of chloride ions in the KURT groundwater solution. These results indicate that SS316L can be used as a canister material in environments similar to those of the KURT groundwater solution (i.e., those involving extremely low concentrations of chloride ions).

Table 4
R_p values of SS316L, Ti-Gr.2, Alloy 22, and Cu exposed to naturally aerated KURT groundwater solution.

	SS316L	Ti-Gr.2	Alloy 22	Cu
R_p [kΩ·cm^2]	3.84×10^2	2.31×10^2	3.23×10^2	2.68×10^1

4. Conclusion

The corrosion behaviors of several canister materials (SS316L, Ti-Gr.2, Alloy 22, and Cu) in KURT groundwater were examined. The corrosion potential and corrosion current of the test materials in

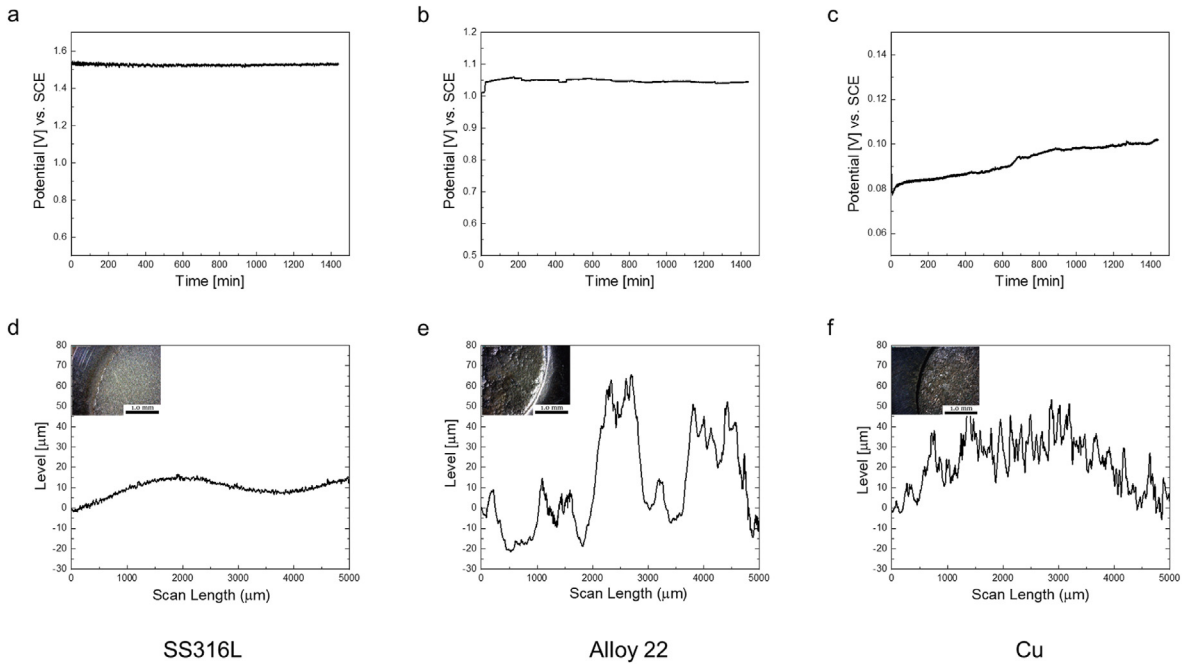

Fig. 5. Potential profiles (a–c) during anodic dissolution and surface roughness profiles (d–f) of SS316L, Alloy 22, and Cu after the dissolution test in the 0.1-M Na_2SO_4 added KURT groundwater solution at 25 °C.

the naturally aerated groundwater solution were measured using the polarization technique. According to impedance measurements, Cu was more susceptible to general corrosion than the other materials, with the polarization resistance of Cu in the groundwater solution being one order lower than those of the other considered materials. The most uniform corrosion from the anodic dissolution in the naturally aerated KURT groundwater solution corresponded to SS316L. Notably, this research was based on short-term electrochemical techniques. Future work can be aimed at examining the complex and long-term behaviors of materials to assess canister materials and ensure their safety in Korean domestic repository environments. Furthermore, it is also necessary to investigate the complex interactive behavior between buffer materials and several candidate canister materials suggested by this research for the entire safety assessment of disposal system.

Declaration of competing interest

The authors declare that they have no known competing financial interests or personal relationships that could have influenced the work reported in this paper.

Acknowledgements

This work was supported by the Institute for Korea Spent Nuclear Fuel (iKSNF) and the National Research Foundation of Korea (NRF) grant funded by the Korea government (Ministry of Science and ICT, MSIT) (2021M2E1A1085193, 2021M2E3A2041351).

References

[1] SKB, Design Premises for a KBS-3V Repository Based on Results from the Safety Assessment SR-Can and Some Subsequent Analyses, Svensk Kärnbränslehantering AB, TR-09–22, 2009.
[2] R. Gubner, U. Andersson, Corrosion Resistance of Copper Canister Weld Material, Svensk Kärnbränslehantering AB, TR-07–07, 2007.
[3] T. Hedman, A. Nystrom, C. Thegerstrom, Swedish containers for disposal of spent nuclear fuel and radioactive waste, C. R. Physique 3 (2002) 903–913.
[4] F. King, L. Ahonen, C. Taxen, U. Vuorinen, L. Werme, Copper Corrosion under Expected Conditions in a Deep Geological Repository, Svensk Kärnbränslehantering AB, TR-01–23, 2001.
[5] F. King, C. Lilja, M. Vähänen, Progress in the understanding of the long-term corrosion behavior of copper canisters, J. Nucl. Mater. 438 (2013) 228–237.
[6] P. Jakupi, D. Zagidulin, J.J. Noel, D.W. Shoesmith, The impedance properties of the oxide film on the Ni-Cr-Mo Alloy-22 in neutral concentrated sodium chloride solution, Electrochim. Acta 56 (2011) 6251–6259.
[7] F. King, C. Padovani, Review of the corrosion performance of selected canister materials for disposal of UK HLW and/or spent fuel, Corrosion Eng. Sci. Technol. 46 (2) (2011) 82–90.
[8] F. King, Waste containers, Compr. Nucl. Mater. 2 (2012) 421–450.
[9] DOE, Yucca Mountain Repository License Application, US Department of Energy, DOE/RW-0573, 2008.
[10] M. Ochoa, M.A. Rodríguez, S.B. Farina, Corrosion of high purity copper in solutions containing NaCl, Na_2SO_4 and $NaHCO_3$ at difference temperatures, Procedia Mater. Sci. 9 (2015) 460–468.
[11] R. Sandström, R. Wu, Origin of the Extra Low Creep Ductility of Copper without Phosphorous, Svensk Kärnbränslehantering AB, TR-07–02.
[12] F. King, C. Lilja, K. Pedersen, P. Pikänen, M. Vähänen, An Update of the State-Of-The-Art Report on the Corrosion of Copper under Expected Conditions in a Deep Geologic Repository, Svensk Kärnbränslehantering AB, TR-10–67.
[13] L.J. Knob, D.L. Olson, Metals handbook, Corrosion 13 (1987) 669, ninth ed.
[14] P. Refait, J.A. Bourdoiseau, M. Jeannin, D.D. Nguyen, A. Romaine, R. Sabot, Electrochemical formation of carbonated corrosion products on carbon steel in deaerated solutions, Electrochim. Acta 79 (2012) 210–217.
[15] H. Luo, H. Su, B. Li, G. Ying, Electrochemical and passive behavior of tin alloyed ferritic stainless steel in concrete environment, Appl. Surf. Sci. 439 (2018) 232–239.
[16] A. Bacelis, L. Veleva, M.A. Alpuche-Avilés, Copper corrosion behavior in simulated concrete-pore solutions, Metals 10 (4) (2020) 474–493.
[17] A.M. Fekry, R.M. El-Sherif, Electrochemical corrosion behavior of magnesium and titanium alloys in simulated body fluid, Electrochim. Acta 54 (2009) 7280–7285.
[18] Q. Zhang, M. Zhen, Y. Huang, H.J. Kunte, X. Wang, Y. Liu, C. Zheng, Long term corrosion estimation of carbon steel, titanium and its alloy in backfill material of compacted bentonite for nuclear waste repository, Sci. Rep. 9 (2019) 3195–3212.
[19] B. Rosborg, T. Kosec, A. Kranjc, J. Pan, A. Legat, Electrochemical impedance spectroscopy of pure copper exposed in bentonite under oxic conditions, Electrochim. Acta 56 (2011) 7861–7870.
[20] I.D. Raistrick, J.R. MacDonald, D.R. Francschetti, Chapter 2, in: J.R. MacDonald (Ed.), Impedance Spectroscopy: Emphasizing Solid Materials and Systems, John Wiley & Sons, New York, 1987.
[21] Y. Van Ingelgem, A. Hubin, J. Vereecken, Investigation of the first stages of the localized corrosion of pure copper combining EIS, FE-SEM and FE-AES, Electrochim. Acta 52 (2007) 7642–7650.
[22] W.A. Badawy, K.M. Ismail, A.M. Fathi, Effect of Ni content on the corrosion

behavior of Cu-Ni alloys in neutral chloride solutions, Electrochim. Acta 50 (2005) 3603–3608.
[23] J.-P. Diard, J.-M. Le Canut, B. Le Goreec, C. Montella, Copper electrodissolution in 1 M HCl at low current densities. II. Electrochemical impedance spectroscopy study, Electrochim. Acta 43 (1998) 2485–2501.
[24] A.M. Fenelon, C.B. Breslin, The electrochemical synthesis of polypyrrole at a copper electrode: corrosion protection properties, Electrochim. Acta 47 (2002) 4467–4476.
[25] E.M. Sherif, S.-M. Park, Inhibition of copper corrosion in 3.0% NaCl solution by *N*-phenyl-1,4-phenylenediamine, J. Electrochem. Soc. 152 (2005) B428–B433.
[26] T. Tüken, B. Yazici, M. Erbil, The use of polyindole for prevention of copper corrosion, Surf. Coat. Technol 200 (2006) 4802–4809.
[27] K. Rahmouni, M. Keddam, A. Srhiri, H. Takenouti, Corrosion of copper in 3% NaCl solution polluted by sulphide ions, Corros. Sci. 47 (2005) 3249–3266.
[28] G. Cicileo, B. Rosales, F. Varela, J. Vilche, Comparative study of organic inhibitors of copper corrosion, Corros. Sci. 41 (1999) 1359–1375.
[29] A. Palit, S.O. Pehkonen, Copper corrosion in distribution systems: evaluation of a homogeneous Cu_2O film and a natural corrosion scale as corrosion inhibitors, Corros. Sci. 42 (2000) 1801–1822.
[30] B. Trachli, M. Keddam, H. Takenouti, A. Srhiri, Protective effect of electropolymerized 3-amino 1,2,4-triazole towards corrosion of copper in 0.5 M NaCl, Corros. Sci. 44 (2002) 997–1008.
[31] M.B. Valcarce, S.R. De Sánchez, M. Vázquez, A comparative analysis of copper and brass surface films in contact with tap water, J. Mater. Sci. 41 (2006) 1999–2007.
[32] A. Srivastava, R. Balasubramaniam, Microstructural characterization of copper corrosion in aqueous and soil environments, Mater. Charact 55 (2005) 127–135.
[33] F. Brizuela, R. Procaccini, S. Cere, M. Vazquez, Anodically grown films on copper and copper-nickel alloys in slightly alkaline solutions, J. Appl. Electrochem. 36 (2006) 583–590.
[34] M. Galai, H. Benqlilou, M.E. Touhami, T. Belhaj, K. Berrami, H. El Kafssaoui, Comparative analysis for the corrosion susceptibility of copper alloys in sandy soil, Environ. Eng. Res. 23 (2018) 164–174.